Three-pathway electromagnetically induced transparency and absorption based on coupled superconducting resonators

Tianning Zheng [1,*] Pengqi Wang,[1] Bin Wei,[2] Boyu Lu,[2] Bisong Cao,[2] and Fuchuan Lei [3,†]

[1]*Fert Beijing Institute, MIIT Key Laboratory of Spintronics, School of Integrated Circuit Science and Engineering, Beihang University, Beijing 100191, China*

[2]*Department of Physics, State Key Laboratory of Low-Dimensional Quantum Physics, Tsinghua University, Beijing 100084, China*

[3]*School of Physics, Northeast Normal University, Changchun 130024, China*

(Received 4 September 2023; accepted 13 October 2023; published 2 November 2023)

Electromagnetically induced transparency (EIT) and electromagnetically induced absorption (EIA) have many applications, especially for achieving slow light and fast light. EIT and EIA have been widely observed in both quantum and classical systems where two transition pathways could interference destructively or constructively. Multipathway interference has been a concern in recent works, however, due to the difficulty of precisely controlling the system parameters, the experimental study of multipathway interference is generally challenging. In this paper, we explore a coupled high-temperature-superconducting (HTS) resonator platform for implementing three-pathway electromagnetically induced transparency (TEIT) and absorption (TEIA). In our system, both resonant frequencies and linewidths (loss) of each resonator as well as their coupling strength can be precisely controlled, thus TEIT and TEIA can be implemented as a set. Our proposed method shows great potential for use in microwave signal processing in the future, such as slow wave, fast wave, and radio-frequency memory. Our results indicate the HTS resonator is an ideal platform for investigating versatile coherent phenomena.

DOI: 10.1103/PhysRevA.108.053105

I. INTRODUCTION

Electromagnetically induced transparency (EIT) is a significant coherent phenomenon in both classical and quantum physics, resulting from the out-of-phase interference between two pathways [1]. EIT was first developed in gas vapor atom systems [2] based on the theory of quantum coherence between two transition pathways to the same energy level in a three-level system. After that, EIT has been demonstrated in numerous classical physics systems due to its similar interference properties to atomic systems. As a result, many easily controllable classical physics systems have been developed such as metamaterials [3–8], plasma [9–12], optomechanics [13–17], microresonators [18–20], and superconductors [21–24] etc.

Up to now, most studies of EIT and electromagnetically induced absorption (EIA) have focused on the simplest case, which involves interference between two pathways. However, by generalizing this to three-pathway or multipathway interference, new phenomena based on four-level or multilevel atomic schemes can be achieved. These phenomena not only deepen our understanding of quantum and classical coherence theory, but also enable us to manipulate light and electromagnetic waves in new ways, such as double EIT and double EIA transitions, observed in controllable photonic molecules [25] and multi-EIT and EIA in optical microresonators [26], where two or more peaks/dips with approximately the same linewidth appear within a broad absorption/transparency background. If we further tailor the linewidths and resonant frequencies of the modes, we can observe another type of EIT or EIA, known as three-pathway electromagnetically induced transparency (TEIT) and three-pathway electromagnetically induced absorption (TEIA) [27,28]. Achieving effective multipathway interference requires precise control of the system parameters, as more freedoms are involved than simple two-pathway interference.

In this paper, we propose and experimentally implement TEIT and TEIA in a microwave regime based on three coupled high-temperature-superconducting (HTS) resonator systems. We use Y-Ba-Cu-O (YBCO) film as the superconducting material which ensures achieving high Q modes [29]. Another advantage of using HTS is that their resonant frequencies can be mechanically tuned without sacrificing Q value, and the coupling strength between the resonators can be precisely designed by means of numerical simulations. This work shows the potential of HTS for experimentally studying multimode physics, while the realization of TEIT and TEIA would facilitate the understanding of coherence phenomena.

II. DESIGN AND ANALYSIS

Figures 1(a) and 1(b) illustrate the schematic diagrams for achieving TEIT and TEIA based on coupled superconducting resonators. We design two coupled-resonator configurations, both of which are composed of a low-Q resonator (R1), a medium-Q resonator (R2), and a high-Q resonator (R3). Meanwhile, a feedline connecting the source input and the microwave signal output, is coupled to R1 in both configurations.

*zhengtn@buaa.edu.cn
†fuchuanlei@nenu.edu.cn

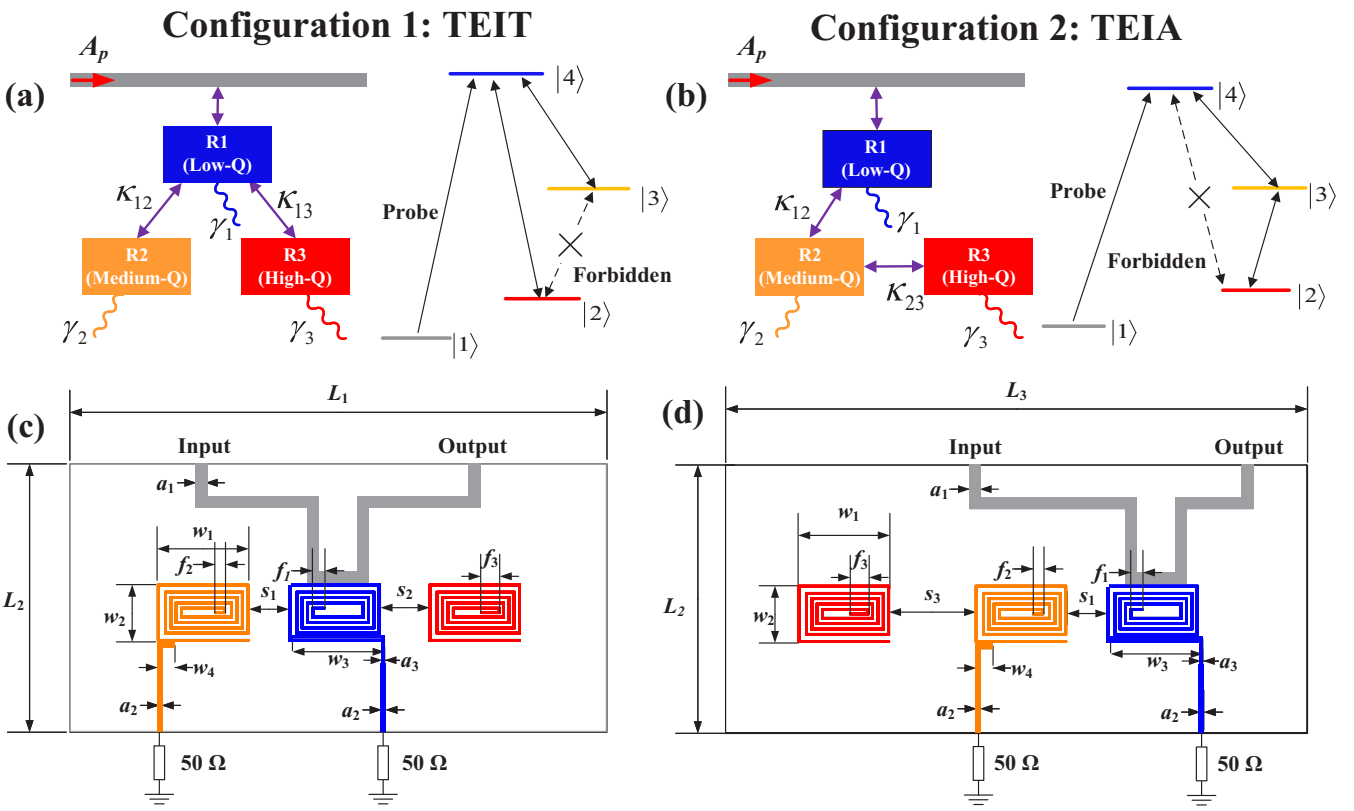

FIG. 1. (a), (b) Schematic and (c), (d) circuit diagrams of three-coupled-resonator based TEIT and TEIA. The patterns are fabricated on YBCO films. The YBCO film has a conductivity of 1.2×10^{14} S/m, and a thickness of 600 nm. The substrate is MgO with a thickness of 0.5 mm, and its relative permittivity is 9.7. The depth of the air layer below the top cover is 5 mm. The dimensions in the circuit are as follows: $L_1 = 24$ mm, $L_2 = 12$ mm, $L_3 = 26$ mm, $a_1 = 0.48$ mm, $a_2 = 0.2$ mm, $a_3 = 0.08$ mm, $w_1 = 4.08$ mm, $w_2 = 2.56$ mm, $w_3 = 4.02$ mm, $w_4 = 0.74$ mm, $s_1 = 1.8$ mm, $s_2 = 2.2$ mm, $s_3 = 3.84$ mm, $f_1 = 0.56$ mm, $f_2 = 0.48$ mm, $f_3 = 0.86$ mm. The linewidth and line spacing are both 0.08 mm in the spiral resonators.

TEIT is implemented with configuration 1, where R2 and R3 are directly coupled to R1 but there is no coupling between them. However, in configuration 2, which implements TEIA, the feedline, R1, R2, and R3 are coupled in a cascaded way without any other nonadjacent cross couplings.

In the circuits, a HTS spiral resonator is utilized for its compact size [30]. All the resonators are working at half-wavelength resonance mode with a fundamental frequency of 1305 MHz. A transmission line, coupled with the resonator at one end and connected to a 50 Ω impedance at the other end, is introduced to realize Q-factor management for R1 and R2. The coupling strength between two adjacent resonators can be adjusted by controlling their distance. The microwave signal is fed from the input port at the left end, and the output response is measured at the right end of the feedline. The two circuits are both achieved at a compact chip size with dimensions smaller than 26 mm × 12 mm, which amounts to $0.011\lambda_0 \times 0.005\lambda_0$, where λ_0 is the wavelength of the microwave in free space.

TEIT and TEIA can be qualitatively explained as three-pathway interference, as shown in Figs. 1(a) and 1(b). In a weak-coupling regime, the model can be described as a four-level system, which consists of one ground state and three bare states with distinct decay rates. In configuration 1, there are three transition pathways to reach state $|4\rangle$ from state $|1\rangle$, including one direct pathway, $|1\rangle \rightarrow |4\rangle$ (denoted as P11), and two indirect pathways, $|1\rangle \rightarrow |4\rangle \rightarrow |2\rangle \rightarrow |4\rangle$ (denoted as P12) and $|1\rangle \rightarrow |4\rangle \rightarrow |3\rangle \rightarrow |4\rangle$ (denoted as P13). In a weak-coupling regime, P11 has a π phase difference from both P12 and P13, therefore giving rise to two superposed transparency peaks with different linewidths in the absorption window, corresponding to TEIT. In configuration 2, the bare states remain the same but the pathways change to $|1\rangle \rightarrow |4\rangle$ (denoted as P21), $|1\rangle \rightarrow |4\rangle \rightarrow |3\rangle \rightarrow |4\rangle$ (denoted as P22), and $|1\rangle \rightarrow |4\rangle \rightarrow |3\rangle \rightarrow |2\rangle \rightarrow |3\rangle \rightarrow |4\rangle$ (denoted as P23), whose phase differences are quite different from configuration 1. In this situation, as the pathway gets "longer," a phase of π is added one by one to P22 and P23, therefore P21 and P22 are antiphase but P21 and P23 are in phase, giving rise to a broad transparency peak and a narrow absorption dip superposed in the absorption window—this is TEIA.

To understand these phenomena in an alternative quantitative way, i.e., dressed-state picture, we can formulate the transmission amplitude as the form of a superposition of eigenmodes. According to coupled-mode theory, the steady state of the two configurations can be expressed as follows [25,31],

$$\begin{pmatrix} \Omega_1 & -\kappa_{12} & -\kappa_{13} \\ -\kappa_{12} & \Omega_2 & -\kappa_{23} \\ -\kappa_{13} & -\kappa_{23} & \Omega_3 \end{pmatrix} \begin{pmatrix} A_1 \\ A_2 \\ A_3 \end{pmatrix} = \begin{pmatrix} -i\sqrt{\gamma_e} A_p \\ 0 \\ 0 \end{pmatrix}, \quad (1)$$

TABLE I. Parameters of models describing the two configurations.

	Configuration 1	Configuration 2
γ_c (MHz)	$2\pi \times 1.06$	$2\pi \times 1.06$
γ_1 (MHz)	$2\pi \times 17.06$	$2\pi \times 17.06$
γ_2 (MHz)	$2\pi \times 0.52$	$2\pi \times 0.52$
γ_3 (MHz)	$2\pi \times 0.007$	$2\pi \times 0.007$
ω_1 (MHz)	$2\pi \times 1305$	$2\pi \times 1305$
ω_2 (MHz)	$2\pi \times 1305$	$2\pi \times 1305$
ω_3 (MHz)	$2\pi \times 1305$	$2\pi \times 1305$
κ_{12} (MHz)	$2\pi \times 1.153$	$2\pi \times 1.153$
κ_{13} (MHz)	$2\pi \times 0.48$	0
κ_{23} (MHz)	0	$2\pi \times 0.16$

where A_i $(i = 1, 2, 3)$ denotes the field amplitudes in R1, R2, and R3, respectively, and A_p is the input field amplitude from the waveguide. $\Omega_i = (\omega - \omega_i) + i\gamma_i/2$, and γ_c represents the total loss rate in R1, R2, and R3, respectively. It is worth mentioning that γ_1 includes the intrinsic loss and the coupling loss with the feedline as well, while γ_2 and γ_3 only describe the intrinsic losses. ω is the frequency of the probe microwave field, while ω_i denotes the resonance frequencies of the three HTS resonators. κ_{ij} denotes the coupling coefficient between two HTS resonators with their numbers accordingly. The output field is given as $A_{\text{out}} = A_p + \sqrt{\gamma_c}A_1$ and the transmission amplitude is $t = A_{\text{out}}/A_p$, the modulus of which $|t|$ is defined as the transmission spectrum which can be measured in the experiment.

Configurations 1 and 2 can be described by the above model with $\kappa_{23} = 0$ and $\kappa_{13} = 0$, respectively. Then, we can get the transmission amplitude and in the form of the superposition of eigenmodes,

$$t_1 = 1 - \frac{i\Omega_2\Omega_3\gamma_c}{(\omega-\omega_{11})(\omega-\omega_{12})(\omega-\omega_{13})} = 1 + \frac{C_{11}}{(\omega-\omega_{11})} + \frac{C_{12}}{(\omega-\omega_{12})} + \frac{C_{13}}{(\omega-\omega_{13})}, \quad (2)$$

$$t_2 = 1 - \frac{i(\Omega_2\Omega_3 - \kappa_{23}^2)\gamma_c}{(\omega-\omega_{21})(\omega-\omega_{22})(\omega-\omega_{23})} = 1 + \frac{C_{21}}{(\omega-\omega_{21})} + \frac{C_{22}}{(\omega-\omega_{22})} + \frac{C_{23}}{(\omega-\omega_{23})}, \quad (3)$$

where C_{1i} and C_{2i} are constants to be determined by equating the corresponding coefficients. The eigenfrequencies of configurations 1 and 2 are denoted by ω_{1i} and ω_{2i}, respectively. Therefore, both transmission spectra can be understood as the superposition of three dressed modes formed by coupling between bare modes.

In our proposed circuits above in Figs. 1(c) and 1(d), the parameters of the models describing the two configurations are shown in Table I. The resonance frequencies of all the resonators are designed with the same value of 1305 MHz. The losses in R3, R2, and R1 are designed to increase at least one order of magnitude one by one and the couplings between resonators are relatively weak, which guarantees no splitting appears.

Although the quadratic equations for the two-coupled-resonator system can be solved easily [31], it is much more difficult to solve the cubic equations analytically. Thus, we apply a comprised method by substituting the numerical parameters in Table I into Eqs. (2) and (3). As mentioned above, the results can be explained by the superposition of three modes on R1 coupling with the feedline. As shown in Fig. 2, the three dressed modes in the two configurations, all centered at 1305 MHz, are denoted as $|h\rangle$, $|m\rangle$, and $|l\rangle$ in descending order of losses in configurations 1 and 2, respectively. The signs before each fraction in Eqs. (2) and (3) indicate the phase of each mode during overlapping. To make it clear, we illustrate the absolute field strength of the three modes as functions of frequency in Figs. 2(b) and 2(e). Modes $|h\rangle$ and $|m\rangle$ in the two configurations are both completely out of phase, producing a relatively wide transparency window in an absorption dip. It is the phase of the third mode $|l\rangle$ dominating the transmission response to be TEIT or TEIA. TEIT and TEIA happen with different superposing phases of the three modes as shown in Figs. 2(b) and 2(e): In configuration 1, modes $|h\rangle$ are antiphase with $|m\rangle$ but in phase with $|l\rangle$, giving rise to TEIT; however in configuration 2, modes $|h\rangle$ are antiphase with $|m\rangle$ and $|l\rangle$ simultaneously, resulting in TEIA. TEIT and TEIA are demonstrated clearly from the calculated transmission spectra as shown in Figs. 2(c) and 2(f), respectively. In the absorption window, there is a transmission peak, within which appears another transmission peak or dip for TEIT and TEIA, respectively.

III. EXPERIMENTAL RESULTS AND DISCUSSION

The circuit is fabricated on two separate MgO substrates with double-side coated YBCO HTS thin films. The fabrication of our proposed devices is similar to the manufacturing of semiconductor chips, which involves photolithography and ion-beam etching as shown in Fig. 3(a). The circuits are then mounted on a metal carrier and are assembled into a shield box as shown in Fig. 3(b). The photographs of the samples are shown in Fig. 3(c). Sapphire tuning screws are mounted on the top cover to correct the fabrication errors just the same as we did in a previous work [29]. The circuits are then tuned to correct the fabrication errors and the center frequencies of the resonators are altered to achieve TEIT and TEIA responses. The circuits are measured with an Agilent N5230C vector network analyzer with an input power of 0 dBm at 65 K. The cryogenic condition is provided by a commercial portable Stirling cryocooler with an output power of 6 W. The measured results of transmission spectra are shown in Fig. 3(d). TEIT and TEIA are clearly shown on the measured results, and the observed transmission spectra are asymmetric due to nonadjacent coupling between the three resonators. In the model we constructed, nonadjacent coupling between the resonators was neglected because the focus of this experiment was on the transmission and absorption produced at the resonance frequencies. Overall, the experimental results are in good agreement with the theoretical model. In addition, the group delays of the two circuits are measured as well, shown in Fig. 3(e). In the TEIT circuit, a slow wave effect is observed as the group delay reaches a positive value of 226 ns. However, in the TEIA circuit, the group delay is −117 ns, indicating a fast wave effect. These results demonstrate that

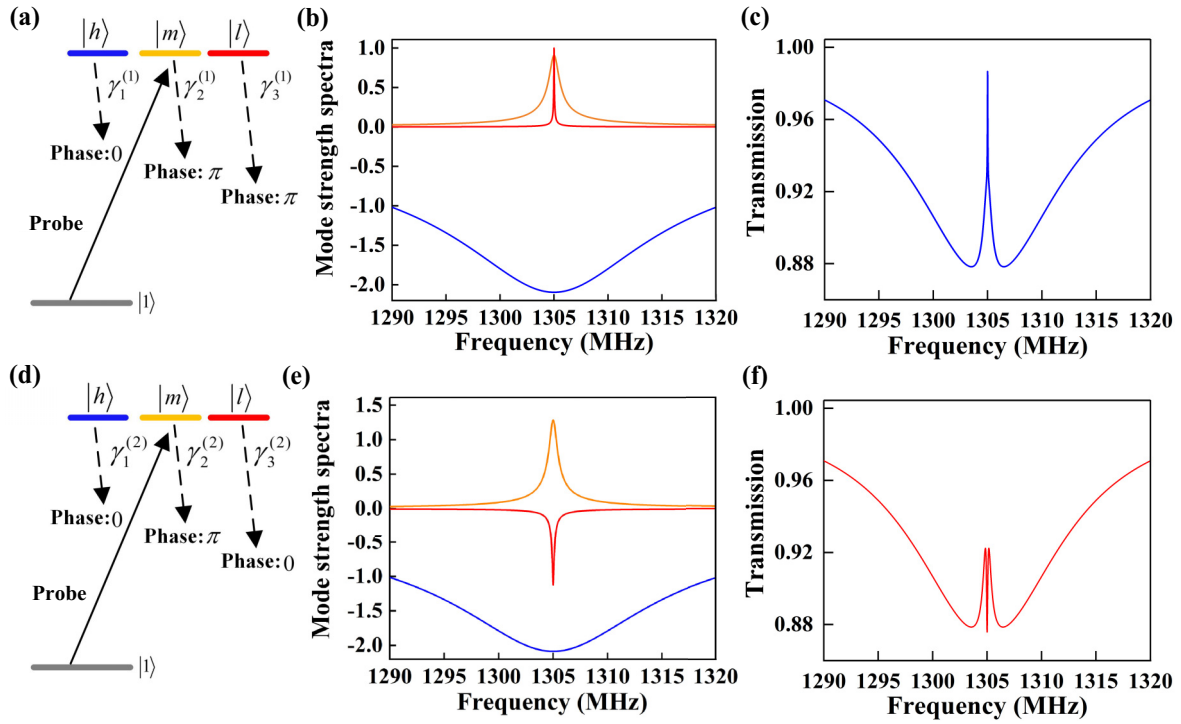

FIG. 2. Dressed-state description of TEIA and TEIA. (a) Three dressed states. (b) Calculated mode strengths in Eq. (2). (c) Transmission spectrum for TEIT. (d)–(f) Same for the case in (a)–(c) but for TEIA. The calculated parameters are $\omega_{11} = 1305 - 8.34i$, $\omega_{12} = 1305 - 0.44i$, $\omega_{13} = 1305 - 0.02i$, $\omega_{21} = 1305 - 8.37i$, $\omega_{22} = 1305 - 0.35i$, $\omega_{23} = 1305 - 0.08i$, $C_{11} = -17.18i$, $C_{12} = 0.40i$, $C_{13} = 0.02i$, $C_{21} = -17.41i$, $C_{22} = 0.45i$, $C_{23} = -0.09i$.

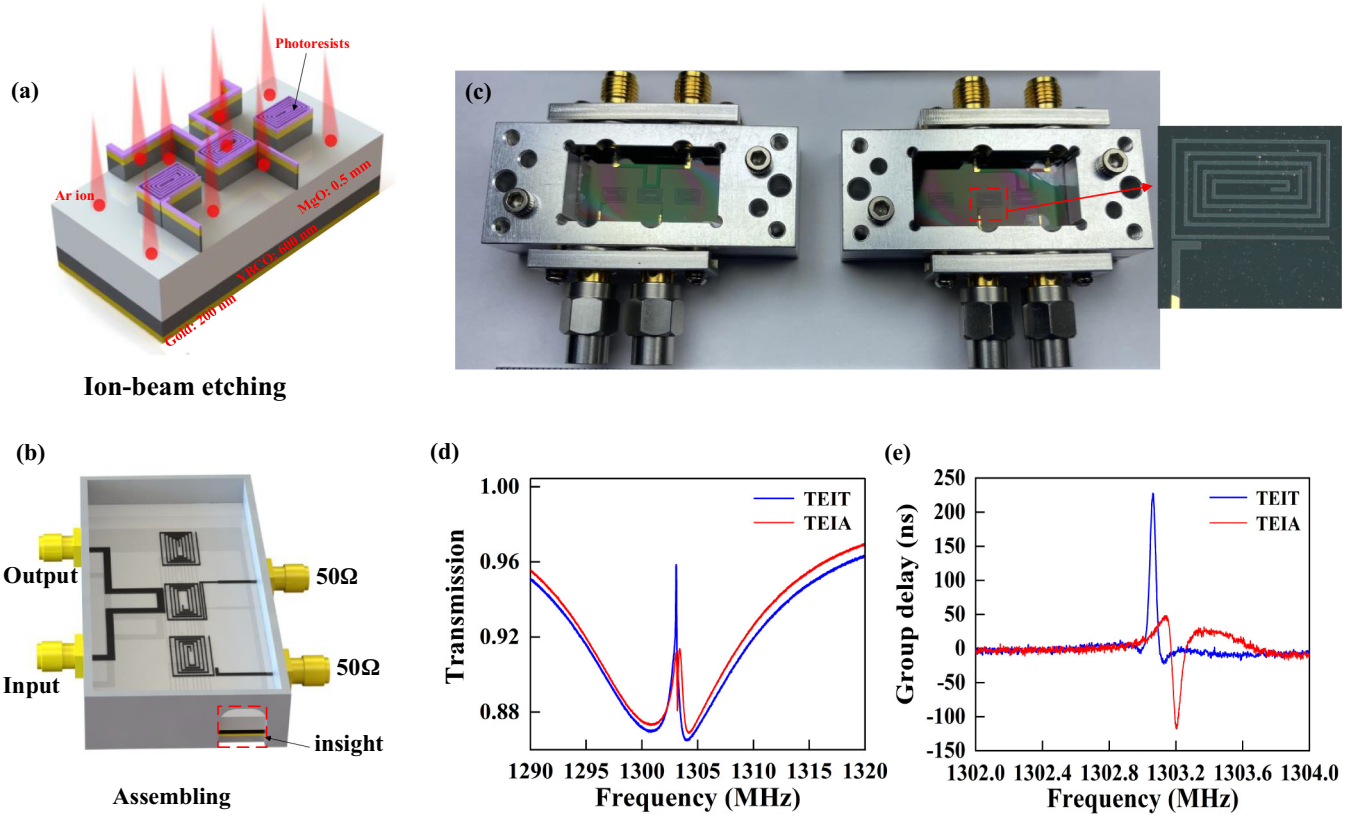

FIG. 3. Experimental demonstration of TEIT and TEIA. Schematic diagram of the (a) fabrication and (b) assembling process. (c) Photograph of the fabricated samples. (d) Measured transmission spectra and (e) group delays for the circuits with configuration 1 and configuration 2.

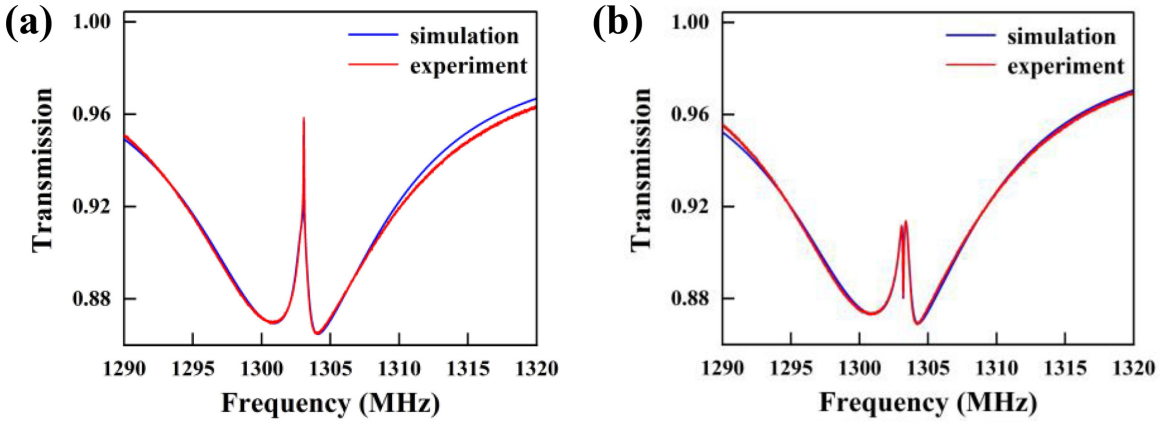

FIG. 4. Measured transmission spectra of the circuits with configurations 1 and 2, implementing (a) TEIT and (b) TEIA, respectively. The parameters for (a) are $\omega_1 = 2\pi \times 1302.1$ MHz, $\omega_2 = 2\pi \times 1303.07$ MHz, $\omega_3 = 2\pi \times 1303.07$ MHz, $\gamma_1 = 2\pi \times 15.9$ MHz, $\gamma_2 = 2\pi \times 0.6$ MHz, $\gamma_3 = 2\pi \times 0.0225$ MHz, $\gamma_{c1} = 2\pi \times 1.06$ MHz, $\gamma_{c2} = 2\pi \times 0.002\,15$ MHz, $\gamma_{c3} = 0$, and for (b) they are $\omega_1 = 2\pi \times 1302$ MHz, $\omega_2 = 2\pi \times 1303.39$ MHz, $\omega_3 = 2\pi \times 1303.2$ MHz, $\gamma_1 = 2\pi \times 16$ MHz, $\gamma_2 = 2\pi \times 0.628$ MHz, $\gamma_3 = 2\pi \times 0.0001$ MHz, $\gamma_{c1} = 2\pi \times 1.06$ MHz, $\gamma_{c2} = 2\pi \times 0.002\,98$ MHz, $\gamma_{c3} = 2\pi \times 0.0002$ MHz.

the proposed method is a convenient way for controlling the speed of microwaves.

Different from the simulation, we note the measured transmission spectra are slightly asymmetric. This can be attributed to two facts: First, there exists non-negligible parasitic coupling between the feedline and resonators R2 and R3, and second, the resonant frequencies of the three resonators are not identical due to a fabrication error. To see its impact, we take into account such coupling, so then Eq. (1) is revised as follows,

$$\begin{pmatrix} \Omega_1 & -\kappa_{12} & -\kappa_{13} \\ -\kappa_{12} & \Omega_2 & -\kappa_{23} \\ -\kappa_{13} & -\kappa_{23} & \Omega_3 \end{pmatrix} \begin{pmatrix} A_1 \\ A_2 \\ A_3 \end{pmatrix} = \begin{pmatrix} -i\sqrt{\gamma_{c1}}A_p \\ -i\sqrt{\gamma_{c2}}A_p \\ -i\sqrt{\gamma_{c3}}A_p \end{pmatrix}, \quad (4)$$

where γ_{c1}, γ_{c2}, and γ_{c3} are the coupling factors between each resonator and the feedline. With proper parameters, we can get a perfect match between theory and measurement [see Figs. 4(a) and 4(b)].

IV. CONCLUSION

In summary, we propose and experimentally demonstrate TEIT and TEIA in a microwave system with three-coupled-HTS resonators. By precisely controlling the resonators' physical parameters, TEIT and TEIA are implemented in two distinct coupled-resonator configurations, where three dressed modes are superposed with different relative phases. It is expected that more interesting phenomena could occur in this three-resonator system if each of the two is mutually coupled. In addition to the three-resonator configuration, our platform also allows more HTS resonators to be integrated, which provides great potential for studying novel optical phenomena, such slow wave, fast wave, and radio-frequency memory, and topologically protected photonic states.

ACKNOWLEDGMENT

This work was supported by National Natural Science Foundation of China (NSFC) (Grant No. 62174010 and No. 12104026) and sponsored by Beijing Nova Program.

[1] S. E. Harris, J. E. Field, and A. Imamoğlu, Nonlinear optical processes using electromagnetically induced transparency, Phys. Rev. Lett. **64**, 1107 (1990).

[2] K.-J. Boller, A. Imamoğlu, and S. E. Harris, Observation of electromagnetically induced transparency, Phys. Rev. Lett. **66**, 2593 (1991).

[3] N. Papasimakis, V. A. Fedotov, N. I. Zheludev, and S. L. Prosvirnin, Metamaterial analog of electromagnetically induced transparency, Phys. Rev. Lett. **101**, 253903 (2008).

[4] P. Tassin, L. Zhang, T. Koschny, E. N. Economou, and C. M. Soukoulis, Low-loss metamaterials based on classical electromagnetically induced transparency, Phys. Rev. Lett. **102**, 053901 (2009).

[5] J. Zhang, S. Xiao, C. Jeppesen, A. Kristensen, and N. A. Mortensen, Electromagnetically induced transparency in metamaterials at near-infrared frequency, Opt. Express **18**, 17187 (2010).

[6] J. Gu, R. Singh, X. Liu, X. Zhang, Y. Ma, S. Zhang, S. A. Maier, Z. Tian, A. K. Azad, H.-T. Chen, A. J. Taylor, J. Han, and W. Zhang, Active control of electromagnetically induced transparency analogue in terahertz metamaterials, Nat. Commun. **3**, 1151 (2012).

[7] P. Tassin, L. Zhang, R. Zhao, A. Jain, T. Koschny, and C. M. Soukoulis, Electromagnetically induced transparency and absorption in metamaterials: The radiating two-oscillator model and its experimental confirmation, Phys. Rev. Lett. **109**, 187401 (2012).

[8] R. Yang, Q. Fu, Y. Fan, W. Cai, K. Qiu, W. Zhang, and F. Zhang, Active control of EIT-like response in a symmetry-broken metasurface with orthogonal electric dipolar resonators, Photonics Res. **7**, 955 (2019).

[9] N. Liu, L. Langguth, T. Weiss, J. Kästel, M. Fleischhauer, T. Pfau, and H. Giessen, Plasmonic analogue of electromagnetically induced transparency at the Drude damping limit, Nat. Mater. **8**, 758 (2009).

[10] R. Taubert, M. Hentschel, J. Kästel, and H. Giessen, Classical analog of electromagnetically induced absorption in plasmonics, Nano Lett. **12**, 1367 (2012).

[11] G. C. Dyer, G. R. Aizin, S. J. Allen, A. D. Grine, D. Bethke, J. L. Reno, and E. A. Shaner, Induced transparency by coupling of Tamm and defect states in tunable terahertz plasmonic crystals, Nat. Photonics **7**, 925 (2013).

[12] C. W. Hsu, B. G. DeLacy, S. G. Johnson, J. D. Joannopoulos, and M. Soljačić, Theoretical criteria for scattering dark states in nanostructured particles, Nano Lett. **14**, 2783 (2014).

[13] G. S. Agarwal and S. Huang, Electromagnetically induced transparency in mechanical effects of light, Phys. Rev. A **81**, 041803(R) (2010).

[14] J. D. Teufel, D. Li, M. S. Allman, K. Cicak, A. J. Sirois, J. D. Whittaker, and R. W. Simmonds, Circuit cavity electromechanics in the strong-coupling regime, Nature (London) **471**, 204 (2011).

[15] P.-C. Ma, J.-Q. Zhang, Y. Xiao, M. Feng, and Z.-M. Zhang, Tunable double optomechanically induced transparency in an optomechanical system, Phys. Rev. A **90**, 043825 (2014).

[16] Y.-P. Gao, Z.-X. Wang, T.-J. Wang, and C. Wang, Optomechanically engineered phononic mode resonance, Opt. Express **25**, 26638 (2017).

[17] H. Xiong and Y. Wu, Fundamentals and applications of optomechanically induced transparency, Appl. Phys. Rev. **5**, 031305(2018).

[18] Q. Xu, S. Sandhu, M. L. Povinelli, J. Shakya, S. Fan, and M. Lipson, Experimental realization of an on-chip all-optical analogue to electromagnetically induced transparency, Phys. Rev. Lett. **96**, 123901 (2006).

[19] K. Totsuka, N. Kobayashi, and M. Tomita, Slow light in coupled-resonator-induced transparency, Phys. Rev. Lett. **98**, 213904 (2007).

[20] C. Wang, X. Jiang, G. Zhao, M. Zhang, C. W. Hsu, B. Peng, A. D. Stone, L. Jiang, and L. Yang, Electromagnetically induced transparency at a chiral exceptional point, Nat. Phys. **16**, 334 (2020).

[21] A. A. Abdumalikov, O. Astafiev, A. M. Zagoskin, Y. A. Pashkin, Y. Nakamura, and J. S. Tsai, Electromagnetically induced transparency on a single artificial atom, Phys. Rev. Lett. **104**, 193601 (2010).

[22] P. M. Anisimov, J. P. Dowling, and B. C. Sanders, Objectively discerning Autler-Townes splitting from electromagnetically induced transparency, Phys. Rev. Lett. **107**, 163604 (2011).

[23] C. Kurter, P. Tassin, L. Zhang, T. Koschny, A. P. Zhuravel, A. V. Ustinov, S. M. Anlage, and C. M. Soukoulis, Classical analogue of electromagnetically induced transparency with a metal-superconductor hybrid metamaterial, Phys. Rev. Lett. **107**, 043901 (2011).

[24] X. Zhou, F. Hocke, A. Schliesser, A. Marx, H. Huebl, R. Gross, and T. J. Kippenberg, Slowing, advancing and switching of microwave signals using circuit nanoelectromechanics, Nat. Phys. **9**, 179 (2013).

[25] C. Yang, X. Jiang, Q. Hua, S. Hua, Y. Chen, J. Ma, and M. Xiao, Realization of controllable photonic molecule based on three ultrahigh-Q microtoroid cavities, Laser Photonics Rev. **11**, 1600178 (2017).

[26] T. Wang, Y.-Q. Hu, C.-G. Du, and G.-L. Long, Multiple EIT and EIA in optical microresonators, Opt. Express **27**, 7344 (2019).

[27] K. Qu and G. S. Agarwal, Phonon-mediated electromagnetically induced absorption in hybrid opto-electromechanical systems, Phys. Rev. A **87**, 031802(R) (2013).

[28] F.-C. Lei, M. Gao, C. Du, Q.-L. Jing, and G.-L. Long, Three-pathway electromagnetically induced transparency in coupled-cavity optomechanical system, Opt. Express **23**, 11508 (2015).

[29] T. Zheng, B. Wei, F. Lei, and B. Cao, Very large group delay in VHF band using coupled high temperature superconducting resonators, Photonics Res. **9**, 1892 (2021).

[30] Y. Zhang, X. Guo, B. Cao, B. Wei, X. Zhang, X. Song, G. Suo, and G. Zhang, An ultracompact superconducting bandpass filter at 40 MHz using spiral resonators and a new feedline structure, IEEE Trans. Appl. Supercond. **22**, 1500205 (2012).

[31] B. Peng, S. K. Özdemir, W. Chen, F. Nori, and L. Yang, What is and what is not electromagnetically induced transparency in whispering-gallery microcavities, Nat. Commun. **5**, 5082 (2014).